# NATIONAL ADVISORY COMMITTEE FOR AERONAUTICS

## **TECHNICAL NOTE 3720**

COMPARISON BETWEEN EXPERIMENTAL AND PREDICTED DOWNWASH

AT A MACH NUMBER OF 0.25 BEHIND A WING-BODY

COMBINATION HAVING A TRIANGULAR WING

OF ASPECT RATIO 2.0

By Norman E. Sorensen and Edward J. Hopkins

Ames Aeronautical Laboratory Moffett Field, Calif.



Washington May 1956

## TECHNICAL NOTE 3720

#### COMPARISON BETWEEN EXPERIMENTAL AND PREDICTED DOWNWASH

AT A MACH NUMBER OF 0.25 BEHIND A WING-BODY

COMBINATION HAVING A TRIANGULAR WING

OF ASPECT RATIO 2.0

By Norman E. Sorensen and Edward J. Hopkins

#### SUMMARY

A study was undertaken to evaluate a method for predicting the downwash in a transverse plane behind a wing-body combination throughout an angle-of-attack range from 0° to 20°. The predicted downwash was calculated by a numerical method in which an array of discrete vortices was allowed to roll up. The wing vortices were assumed to emanate from the trailing edge of the wing with their positions and strengths determined from the measured spanwise distribution of load.

The wing-body combination had a ratio of maximum body diameter to wing span of 0.259, a triangular wing with an aspect ratio of 2.0, and a body of revolution with a fineness ratio of 12.5. Comparisons are made between the experimental and predicted values for the downwash and for the spanwise distribution of load at a Mach number of 0.25. The positions of the vortex cores indicated by the tuft-grid technique, the water-tank technique, and the numerical method are also compared.

The downwash predicted by the numerical method showed general agreement with the experimental downwash at angles of attack up to about 60 to 80. Above these angles considerable disagreement existed between the predicted and experimental downwash. These differences are attributed in part to flow separation effects since flow studies have indicated that the vortex sheet emanates ahead of the wing trailing edge rather than at the wing trailing edge as assumed in the numerical method.

#### INTRODUCTION

Results of a previous investigation in which downwash surveys were made behind six wing-body combinations are presented in reference 1. The downwash is compared therein with that predicted for small angles of attack

by a numerical method which does not account of the vortex sheet. As an extension to the analysis made in reference 1, the present study was undertaken to determine the accuracy with which downwash can be predicted throughout an angle-of-attack range from 0° to 20° by a numerical method similar to that presented in reference 2 in which the vortex sheet was allowed to roll up. A comparison between the predicted and experimental downwash in a transverse plane is presented for the wing-body combination of reference 1 having a ratio of maximum body diameter to wing span of 0.259 and a triangular wing. Visual-flow studies in a wind tunnel and in a water tank were used to indicate the paths of the trailing vortices.

# MODELS AND APPARATUS

The wind-tunnel model from reference 1, used for the downwash and span load comparisons herein, consisted of a body of revolution and a triangular wing having an aspect ratio of 2.0. Maximum ratio of body diameter to wing span was 0.259. Pertinent dimensions of the wing and the body are presented in figure 1. The wing had 63.43° of sweepback at the leading edge and an NACA 0005 section modified as described in reference 1. The multiple-tube survey rake which was attached to the body for the downwash measurements is described in reference 1. The port wing panel had flush orifices in the surface to indicate the surface static pressures. Spanwise locations of these orifices are shown in figure 1. A 1/7-scale model of the wind-tunnel model was employed for the water-tank investigation. However, the wing of the water-tank model had a 0.062-inch-thick flat-plate profile with a rounded leading edge and a sharp trailing edge.

The flow field in a transverse plane was indicated in the wind tunnel by means of a tuft grid similar to the one described in reference 3. The grid consisted of 0.020-inch piano wire drawn tightly over a frame of 3/4-inch steel tubing to form a mesh of 1-inch squares. Intersection points of the wires were soldered and at each of these points a tuft of nylon yarn was attached by means of a 1/2-inch length of linen thread so that the total length of the tuft and thread was about 2-1/2 inches. The nylon tufts were fused at their ends to reduce fraying. During part of the investigation the grid was attached to the body in a plane perpendicular to the body axis at a distance of 0.392 behind the wing trailing edge. This was the same plane as for the downwash surveys of reference 1. For the remainder of the investigation the tuft grid was mounted on a sting support which was attached to the windtunnel survey apparatus as shown in figure 2. Photographs of the tuft grid were taken with a special camera having a lens with a 30-inch focal length which was located 105 feet behind the tuft grid. Measurements of the approximate centers of the circulatory motion indicated by the tufts, considered to be the vortex core centers, were made directly on the photographs. No corrections for parallax were made because of the small error introduced with the camera located so far downstream and the relatively small distance between the tuft grid and the wing trailing edge.

The technique of immersing the model in the water tank, having a diameter of 22 inches, by means of a rack driven at constant speed was the same as used in reference 4, but white "water-soluble" paint was used in place of aluminum powder to indicate the roll up of the vortex sheet. It was found that a thin band of the paint brushed onto the lower surface of the wing near the trailing edge just before immersing the model indicated the roll-up process more clearly than the aluminum powder. The model entered the water at a nearly constant speed for each angle of attack. The entry speeds were reduced at the higher angles of attack to indicate more clearly the roll-up process. For example, at angles of attack of 60 and 200 the entry speeds were approximately 1.0 and 0.2 feet per second, respectively. Roll up of the vortex sheet on the water surface was recorded by motion pictures taken at 64 frames per second. Measurements were made on the photographs of the approximate centers of the two nearly circular areas of white paint in which an accumulation of white paint occurred as time progressed and these centers were considered to correspond to the vortex-core centers.

### TEST CONDITIONS

The downwash measurements, previously presented in reference 1, the tuft-grid studies, and the span load measurements, presented herein, were made in one of the Ames 7- by 10-foot wind tunnels. The downwash and span load measurements were made at a dynamic pressure of 90 pounds per square foot which corresponds to a Mach number of 0.25 and a Reynolds number of 4 million based on the mean aerodynamic chord. To prevent the tufts from blowing downstream or becoming badly frayed, the tuft-grid studies were conducted at a dynamic pressure of 15 pounds per square foot which corresponds to a Mach number of 0.10 and a Reynolds number of 1.6 million. The downwash data were corrected for wind-tunnel wall effects as explained in reference 1. No corrections have been applied to the span load, tuft-grid, or water-tank data. The relationship between the corrected and uncorrected angles of attack for the wind-tunnel model (estimated from ref. 5) is

au .	α
60	6.20
10°	10.3°
14°	14.5°
20°	20.70

An estimate was made of the wind-tunnel wall corrections to the wake displacement in the plane of symmetry for the wind-tunnel model (ref. 1) by the method of reference 6 and for the water-tank model by the method of reference 7. It was found that this correction for the water tank was about 60 percent of the correction for the wind-tunnel model. In either case, application of the correction would shift the vortex sheet (or cores) downward with distance behind the wing trailing edge but not enough to invalidate a qualitative comparison of the vortex-core positions measured by these two techniques.

## METHOD OF PREDICTING VORTEX PATHS AND DOWNWASH

Roll up of the vortex sheets was calculated from an array of doubly infinite line vortices and a doublet which were substituted for the wingbody combination. The wing vortices were assumed to lie initially in a horizontal plane containing the trailing edge of the wing. The initial lateral positions of these wing vortices were determined from the measured spanwise distribution of load on the wing. For each wing vortex there was an image vortex of equal strength positioned within the body so that the boundary condition of no flow through the body was satisfied. The doublet which simulated the body was used to calculate the flow field induced by the body at an angle of attack. Roll up of the vortex sheet was predicted by a stepwise numerical method in which the induced movement of each wing vortex was calculated. The center of gravity of vorticity for those vortices concentrated within a small area was estimated and considered to correspond to the vortex-core centers estimated from the wind-tunnel and water-tank results. After the positions of the wing vortices and their images were established at a particular longitudinal station behind the wing trailing edge, calculations of the downwash were made. These downwash calculations included both a 5-vortex solution and a 10-vortex solution. The notation used throughout this report is defined in Appendix A, and the procedure followed in making the numerical calculations is presented in Appendix B.

## RESULTS AND DISCUSSION

## Span Loading

The distribution of vorticity used in the present downwash calculations was based on the spanwise distribution of load. The distribution of load was determined from pressure measurements on the wing, since it was known from previous investigations on highly swept wings having separated flow

The terminology 5-vortex or 10-vortex solution denotes the number of vortices emanating from the wing trailing edge on either side of the body.

that the spanwise distribution of load cannot be predicted successfully by any known method. The measured span load curves at various angles of attack for a wing incidence of 0° are shown in figure 3. It can be seen in figure 3 that the distribution of load predicted by the method of reference 8 (Weissinger theory with the wing load induced by the body included) for angles of attack of 2° and 6° is quite similar to the measured distribution, but that the magnitude of load is underestimated by this method. At an angle of attack of 10° or above neither the distribution nor the magnitude of load is predicted accurately.

#### Downwash

Experimental downwash angles, presented previously in reference 1, and downwash angles predicted by the numerical method outlined in Appendix B are presented as a function of angle of attack in figure 4. The calculated positions of the vortices at various longitudinal stations behind the wing trailing edge are shown in figure 5 to indicate the amount of roll up of the vortex sheet. It can be seen that a considerable roll up and movement of the vortices has taken place between the wing trailing edge and the downwash survey plane. In general, the downwash predicted from the calculated vortex positions (fig. 5) for  $x_{TE} = 0.39\bar{c}$  agrees with the experimental downwash at angles of attack up to about 6° to 8° (except for z/(b/2) = 0) but disagrees considerably at the high angles of attack as the separation effects become more pronounced. The downwash from the 10-vortex solution generally agrees better with the experimental downwash than the 5-vortex solution at low angles of attack, but no improved agreement is shown at high angles of attack. The large differences in the experimental and predicted downwash at z/(b/2) = 0, even at small angles of attack, can probably be attributed to inaccuracies in the measurements due to the influence of the wing wake and to inaccuracies in the predicted downwash arising from the proximity of the wing trailing vortices to the points at which the predictions were made. It is believed that the lack of agreement at the high angles of attack results primarily from flow separation which causes the vortices to emanate from regions ahead of the wing trailing edge instead of from the wing trailing edge as assumed in the calculations.

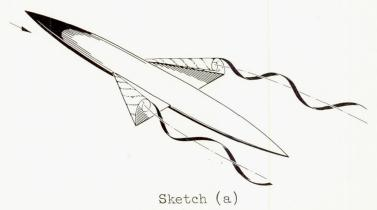
#### Vortex Cores

Measurements on photographs were made of the positions of the vortex cores indicated by the tuft-grid and water-tank techniques for comparisons with the calculated positions. Typical photographs of the flow field and

<sup>2</sup>It was pointed out in reference 8 that the normal forces were underestimated considerably for the same wing-body combination reported upon herein; however, the normal forces were predicted more accurately by the Weissinger method for the other wing-body combinations.

the vortex sheet indicated by the tuft-grid and water-tank techniques are shown in figures 6 and 7 for the wing-body combination. Variations in the vertical and horizontal positions of the vortex cores with longitudinal distance behind the wing trailing edge are presented in figures 8 and 9 for both the wing-body combination and for the wing alone. Tuft grid results from reference 3 are for a wing alone having a plan form similar to the one of the present investigation and are available only for the points at about  $x_{\rm TE}/\bar{c}$  = 0.3 and 1.1.

For the wing-body combination at angles of attack of 6° and 10°, the vertical displacements of the vortex cores from the tuft-grid and water-tank results are in good agreement (see fig. 8). Above an angle of attack of 100 it can be noted that the vertical displacements of the cores for the wing-body combination in the wind tunnel were considerably above those for the combination in the water tank. As the angle of attack increased in the wind tunnel, the tuft-grid results indicate that a vortex core existed at progressively greater distances above the wing trailing edge. For all angles of attack in figure 9, the tuft-grid results indicate that the lateral position of the vortex cores was considerably inward from the wing tips just behind the wing trailing edge and that the cores moved inward only a slight amount with greater distances behind the wing trailing edge. These cores appear to approach asymptotically the centers of gravity of vorticity,  $\overline{y}$ , estimated from the span load curves which are represented by the dashed lines in figure 9. It was found by means of a vortometer3 that the origin of the wing vortex cores occurred near the wing leading edge at the wing-body juncture at angles of attack above 60 and continued downstream. It is postulated that the flow field is as illustrated in sketch (a) below. These vortometer results further substantiate the



previously mentioned positions of the vortex cores indicated by the tuft grid. As shown in figure 9, in the water tank the vortex cores emanate from the wing tips and move inward farther and at a faster rate than those

3A vortometer is an instrument for measuring the size and the paths of vortex cores. This instrument consists of a small circular cylinder which is free to rotate about an axis perpendicular to the axis of the cylinder and which is placed in the flow field with its axis of rotation alined with the free-stream direction.

in the wind tunnel. It appears that a large change in the flow over the wing occurred as the angle of attack increased in the water tank, since the lateral asymptotic positions of roll up moved considerably inward. From the numerical calculations of the formation of the vortex sheet for the 10-vortex solution, the core centers were estimated from results similar to those presented in figure 5 and are also shown in figures 8 and 9. At high angles of attack it is seen that these calculated positions do not agree with the positions measured by either the tuft-grid or the water-tank techniques. These flow-visualization studies indicate that the lack of agreement between the experimental and predicted downwash at high angles of attack is attributable, at least in part, to the faulty assumption made in the calculations that the vortex sheet emanates from the wing trailing edge.

#### CONCLUDING REMARKS

From the comparison between the experimental and predicted results for the wing span load distribution and for the flow field behind a triangular wing-body combination having a wing of aspect ratio 2.0 and a ratio of maximum body diameter to wing span of 0.259, the following remarks can be made:

- l. The predicted spanwise distribution of load at low angles of attack was quite similar to the measured distribution, but at an angle of attack of  $10^{\circ}$  or above, the spanwise distribution of load was not predicted accurately due to flow separation effects.
- 2. In general, the downwash angles predicted by the numerical method, in which the measured spanwise distributions of load and either 5 or 10 wing vortices on each side of the body were used, showed good agreement with the experimental values at small angles of attack up to about 60 and 80. At high angles of attack neither the 5- nor 10-vortex solution gave downwash angles which agreed with the measured downwash angles. This disagreement is partly attributable to the faulty assumption made in the calculations that the vortex sheet emanates from the wing trailing edge. In the wind tunnel the vortex sheet appeared to be shed ahead of the wing trailing edge.
- 3. In general, a comparison of the paths of the vortex cores estimated from the 10-vortex numerical solution, the tuft-grid technique, and the water-tank technique showed progressively less agreement as the angle of attack increased.

Ames Aeronautical Laboratory
National Advisory Committee for Aeronautics
Moffett Field, Calif., Feb. 2, 1956

# APPENDIX A

# NOTATION

Ъ	wing span
b	wing span of exposed panels, b-d
С	local wing chord
ਰ	mean aerodynamic chord, $\frac{\int_0^{b/2} c^2 dy}{\int_0^{b/2} c dy}$
cav	average wing chord, $\frac{c_r}{2}$
cav'	average wing chord of exposed panels, $(1 - \frac{d}{b})c_{av}$
$c_{\mathbf{r}}$	root chord
c <sub>n</sub>	section normal-force coefficient, ger unit span qc
$^{\mathrm{C}}\mathrm{_{L}}$	lift coefficient of exposed wing panels, lift on exposed panels qb'cav'
đ	maximum body diameter
k	number of time increments
n	number of wing vortices
q	free-stream dynamic pressure
R	maximum body radius
t	time
Δt	increment of time
Vo	free-stream velocity

 $(v_h)_m$ lateral velocity perpendicular to the free stream induced at the wing line vortex m by body doublet (positive assumed to the right) lateral velocity perpendicular to the free stream induced at the wing line vortex m by image vortices (positive assumed to the right)  $(v_{\mathbf{W}})_{\mathbf{m}}$ lateral velocity perpendicular to the free stream induced at the wing line vortex m by the wing line vortices (positive assumed to the right) vertical velocity perpendicular to the free stream induced at the wing line vortex m by body doublet (positive assumed down) (w;)m vertical velocity perpendicular to the free stream induced at the wing line vortex m by image vortices (positive assumed down) (WW)m vertical velocity perpendicular to the free stream induced at the wing line vortex m by the wing line vortices (positive assumed down) distance behind the wing trailing edge measured in the horizontal XTE plane passing through the wing trailing edge distance behind the wing trailing edge measured parallel to the XTE, body axis lateral distance from the vertical plane of symmetry У lateral distance from the vertical plane which passes through the y intersection point of the maximum body radius and the wing surface parallel to the vertical plane of symmetry,  $y' = y - \frac{d}{2}$ lateral distance from the vertical plane of symmetry to the Ус vortex core near the wing tip lateral distance from the vertical plane of symmetry to the  $\overline{y}$ center of gravity of vorticity,  $\overline{y} = \frac{\displaystyle\sum_{j=1}^{j} \eta_j \Delta \Gamma_j}{D}$ , considering

the wing vortices on only one side of the body (see sketch (b) of Appendix B for  $\ensuremath{\eta_{\rm j}})$ 

 $\overline{y}$   $\overline{y} - \frac{d}{2}$ 

- z distance perpendicular to the plane of the wing
- z<sub>c</sub> vertical distance from the horizontal plane passing through the wing trailing edge
- α body angle of attack
- max maximum value of circulation assumed positive viewed in the upstream direction for vortices rotating counterclockwise
- $\epsilon$  angle of downwash

## Subscripts

- u uncorrected
- j any wing vortex
- j' image vortex of any wing vortex

## APPENDIX B

## THEORETICAL CONSIDERATIONS

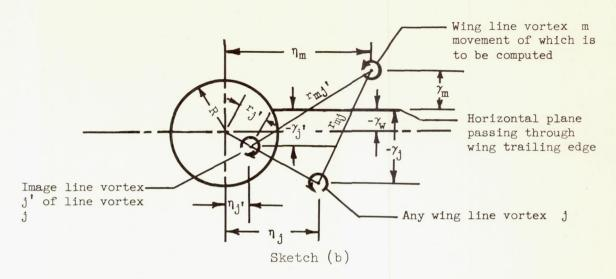
The method and assumptions used for predicting the downwash for the wing-body combination are described below:

The wing was replaced by an array of doubly infinite line vortices and the body was replaced by a doublet. The wing vortices were assumed to lie initially in a horizontal plane passing through the wing trailing edge, and the doublet was assumed to simulate a cylinder having a diameter equal to the maximum diameter of the original body. Each of the wing vortices was assumed to have initial lateral positions governed by the measured distribution of load on the exposed wing panel. To establish the lateral positions of the wing vortices, the span loading curve was replaced by a "stair step" curve having the same enclosed area as the original span loading curve (see fig. 3). The steps were taken at equal increments of loading so that the strength of each of the line vortices was the same. A wing vortex was then located laterally at each step. Image vortices having strengths equal to the wing vortices were positioned within a cylindrical body so that the boundary condition of no flow through its surface was satisfied.

Roll up of the vortex sheet was accounted for by calculation of the displacement of each wing vortex induced by the influence of each of the other vortices in the system. A stepwise process was employed for the displacement calculations in which small time intervals were selected; a suitable interval was found by a number of trials. The resultant induced velocity of a wing line vortex was assumed constant over these selected time intervals. After the positions of the wing vortices were determined at a particular station behind the wing trailing edge, the downwash was calculated by equations similar to those used for the roll-up calculations.

The following sketch defines the symbols not previously defined and can be useful in following the terms given in the equations which follow:

 $<sup>^{1}</sup>$ All distances indicated on sketch (b) are in terms of wing semispans (b/2).



The vertical and horizontal velocities induced by any of the wing line vortices (j) at a given wing-vortex position  $(\gamma_m, \eta_m)$  for a given time interval can be computed from the Biot-Savart equation as:

$$(w_w)_m = \frac{\Gamma_{\text{max}}}{\pi b} \sum_{j=1}^{n} \left(\frac{\Delta \Gamma_j}{\Gamma_{\text{max}}}\right) \left[\frac{\eta_j - \eta_m}{(r_{mj})^2}\right]$$
 (B1)

$$(v_w)_m = \frac{\Gamma_{max}}{\pi b} \sum_{j=1}^{n} \left(\frac{\Delta \Gamma_j}{\Gamma_{max}}\right) \left[\frac{\gamma_j - \gamma_m}{(r_{mj})^2}\right]$$
 (B2)

where the maximum value of circulation  $\Gamma_{\text{max}}$  can be written in terms of the lift coefficient as

$$\Gamma_{\text{max}} = \frac{V_{\text{o}} c_{\text{av}}' c_{\text{L}}}{2 \left(\frac{\overline{y}'}{b/2}\right)}$$
(B3)

Velocities induced by the images of the wing vortices can be calculated by placing the image vortices on radial lines extending from the center of the cylindrical body to each of the wing vortices. The distance along these lines  $r_j$ , measured from the body center to the image vortices can be expressed as

$$r_{j}' = \frac{R^2}{\sqrt{\eta_{j}^2 + (\gamma_{j} - \gamma_{w})^2}}$$
 (B4)

Equations (B1) and (B2) above may be rewritten for the vertical and horizontal velocities induced by the image vortices as

$$(w_{i})_{m} = \frac{\Gamma_{\text{max}}}{\pi b} \sum_{j=1}^{n} \frac{\Delta \Gamma_{j}}{\Gamma_{\text{max}}} \left[ \frac{\eta_{j} - \eta_{m}}{(r_{m}_{j})^{2}} \right]$$
 (B5)

and

$$(v_{i})_{m} = \frac{\Gamma_{\text{max}}}{\pi b} \sum_{j'=1}^{n} \frac{\Delta \Gamma_{j'}}{\Gamma_{\text{max}}} \left[ \frac{\gamma_{j'} - \gamma_{m}}{(r_{m,j'})^{2}} \right]$$
 (B6)

where

$$(r_{mj})^{2} = (\gamma_{j} - \gamma_{m})^{2} + (\eta_{j} - \eta_{m})^{2}$$
 (B7)

and by use of equation (B4)

$$\gamma_{j} = \gamma_{w} + \frac{(\gamma_{j} - \gamma_{w})R^{2}}{\eta_{j}^{2} + (\gamma_{j} - \gamma_{w})^{2}}$$
(B8)

and

$$\eta_{j} = \frac{\eta_{j} R^{2}}{\eta_{j}^{2} + (\gamma_{j} - \gamma_{w})^{2}}$$
(B9)

To account for the velocities induced by the body at an angle of attack, the body was replaced by a doublet and only the component of free-stream velocity perpendicular to the body axis was considered. The expressions for the vertical and horizontal velocities can be derived in the same way as the expressions given in Appendix A of reference 1 and are

$$(w_b)_m = \frac{\sin 2\alpha}{2} V_0 R^2 \left\{ \frac{(\gamma_w - \gamma_m)^2 - \eta_m^2}{[(\gamma_w - \gamma_m)^2 + \eta_m^2]^2} \right\}$$
 (BlO)

and

$$(v_b)_m = -2V_0 R^2 \sin \alpha \left\{ \frac{(\gamma_w - \gamma_m)\eta_m}{[(\gamma_w - \gamma_m)^2 + \eta_m^2]^2} \right\}$$
 (B11)

With an assumed time increment the total vertical and horizontal displacement of a wing line vortex can be computed from the induced velocities given in equations (Bl), (B2), (B5), (B6), (B10), and (B11) as

$$(\gamma_{\rm m})_{\rm total} = \sum_{\rm k=0}^{\rm t/\Delta t} \left\{ \left[ (w_{\rm w})_{\rm m} + (w_{\rm i})_{\rm m} + (w_{\rm b})_{\rm m} \right] \Delta t \right\}_{\rm k}$$
 (B12)

and

$$(\eta_{m})_{\text{total}} = \sum_{k=0}^{t/\Delta t} \left\{ \left[ (v_{w})_{m} + (v_{i})_{m} + (v_{b})_{m} \right] \Delta t \right\}_{k}$$
 (B13)

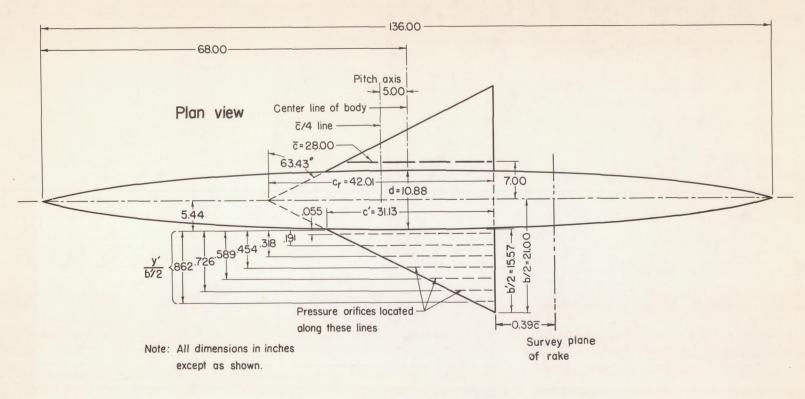
and the distance behind the wing trailing edge in semispans to the transverse plane where downwash is to be calculated is

$$\tau_{\text{TE}} = \frac{V_{\text{O}}t}{b/2} \tag{B14}$$

With the positions of all the line vortices, including the image vortices, calculated at a given distance behind the wing trailing edge  $\tau_{TE}$ , the downwash velocity w was computed from an equation similar to equation (B1). The angle of downwash was then approximated as  $\varepsilon = \text{w/V}_0$ .

#### REFERENCES

- 1. Hopkins, Edward J., and Sorensen, Norman E.: Downwash Survey Behind
  Two Low-Aspect-Ratio Variable-Incidence Wings in Combination With
  Three Different Size Fuselages at a Mach Number of 0.25. NACA
  RM A55A07, 1955.
- 2. Rogers, Arthur William: Application of Two-Dimensional Vortex Theory to the Prediction of Flow Fields Behind Wings of Wing-Body Combinations at Subsonic and Supersonic Speeds. NACA TN 3227, 1954.
- 3. Bird, John D., and Riley, Donald R.: Some Experiments on Visualization of Flow Fields Behind Low-Aspect-Ratio Wings by Means of a Tuft Grid. NACA TN 2674, 1952.
- 4. Spreiter, John R., and Sacks, Alvin H.: The Rolling Up of the Trailing Vortex Sheet and Its Effect on the Downwash Behind Wings. Jour. Aero. Sci., vol. 18, no. 1, Jan. 1951, pp. 21-32, 72.
- 5. Swanson, Robert S., and Gillis, Clarence L.: Wind-Tunnel Calibration and Corrections Procedures for Three-Dimensional Models. NACA WR L-1, 1944. (Supersedes NACA ARR L4E31)
- 6. Swanson, Robert S., and Schuldenfrei, Marvin J.: Jet-Boundary Corrections to the Downwash Behind Powered Models in Rectangular Wind Tunnels with Numerical Values for 7- by 10-Foot Closed Wind Tunnels. NACA WR L-711, 1942.
- 7. Glauert, H.: The Elements of Aerofoil and Airscrew Theory. The MacMillan Company, New York, 1943, p. 190.
- 8. Hopkins, Edward J., and Carel, Hubert C.: Experimental and Theoretical Study of the Interference at Low Speed Between Slender Bodies and Triangular Wings. NACA RM A53Al4, 1953.



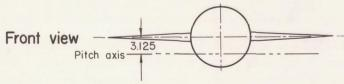
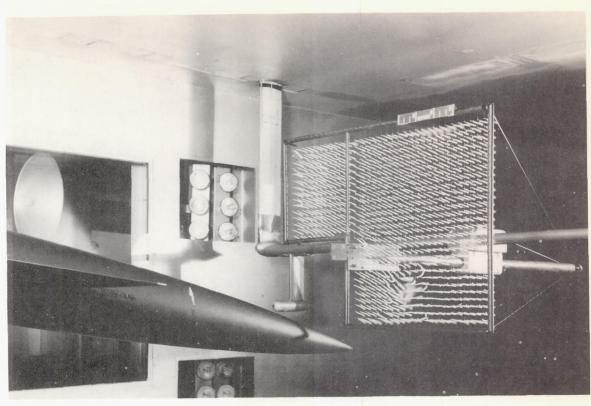


Figure 1.- Dimensional sketch of the wing-body combination.



A-20359

Figure 2.- The tuft grid mounted on the wind-tunnel survey apparatus.

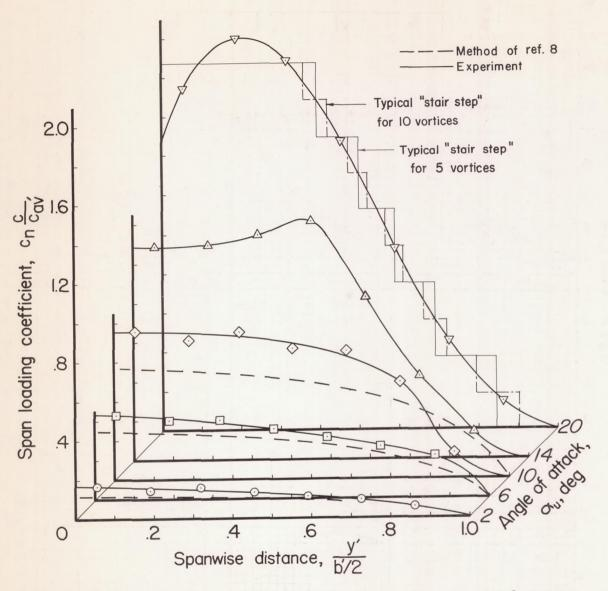


Figure 3.- Effect of angle-of-attack change on the span load curves.

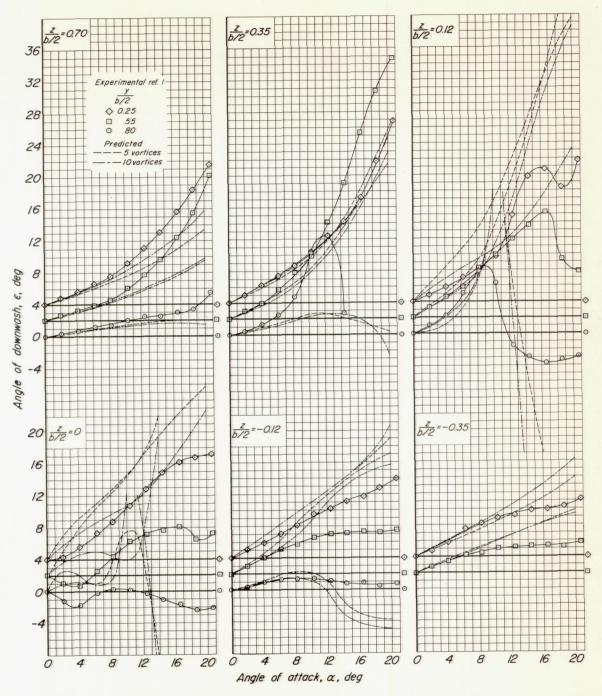


Figure 4.- Comparison of experimental downwash with downwash predicted by the numerical method of Appendix B ( $x_{TE}^{\ell} = 0.39\bar{c}$ ).

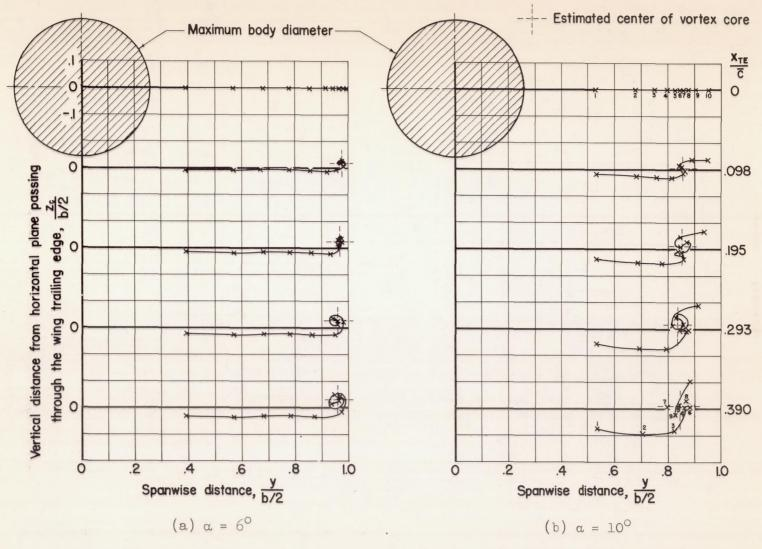


Figure 5.- Roll up of the vortex sheet predicted by the numerical method of Appendix B (10-vortex solution) with estimated center of vortex cores.

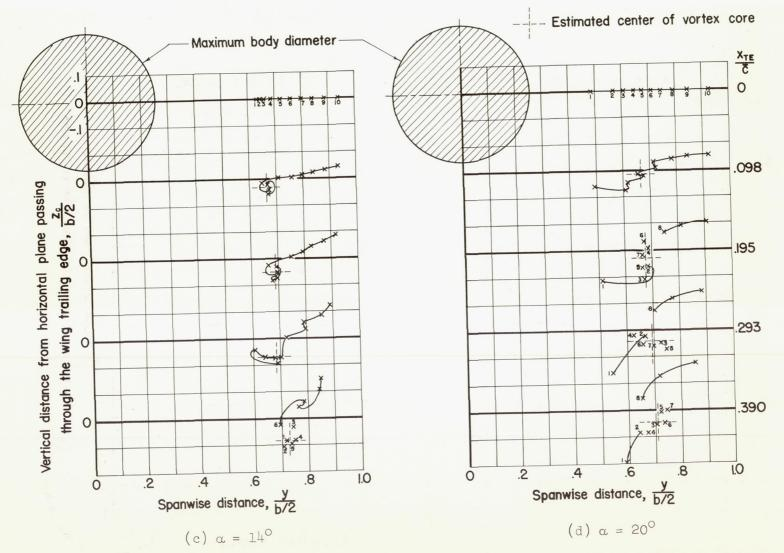
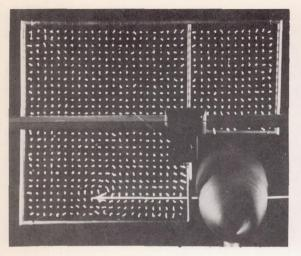
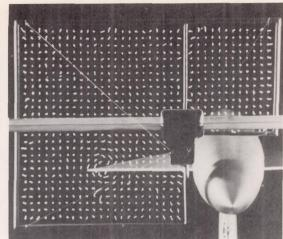


Figure 5.- Concluded.

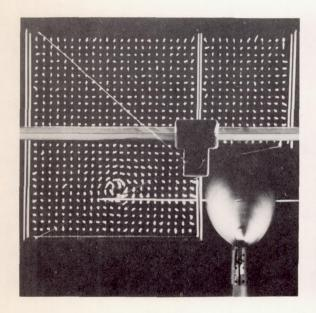
23

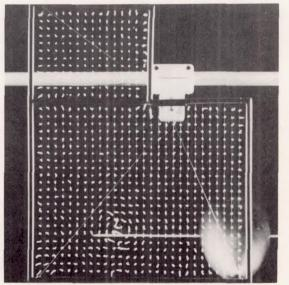




 $x_{TE} = 0.2\overline{c}$ 

 $x_{TE} = 1.0\bar{c}$ 



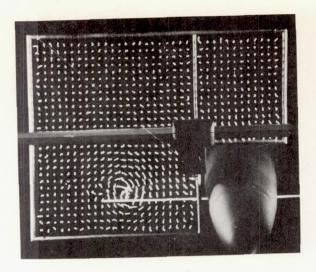


 $x_{TE} = 1.6\bar{c}$ 

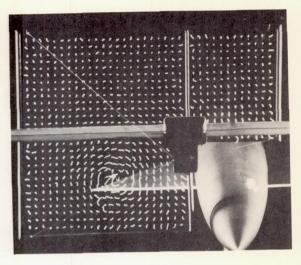
 $x_{TE} = 3.2\overline{c}$ 

(a) 
$$\alpha_{\rm u} = 6^{\rm o}$$

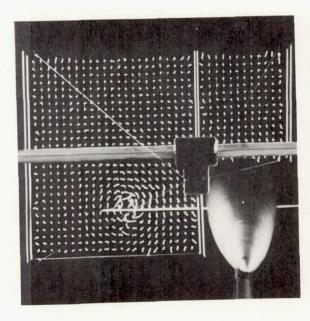
Figure 6.- Typical flow fields indicated by tuft grid at various angles of attack.



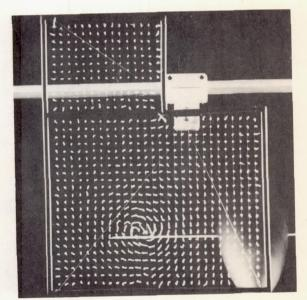
 $x_{TE} = 0.2\overline{c}$ 



 $x_{TE} = 1.0\overline{c}$ 



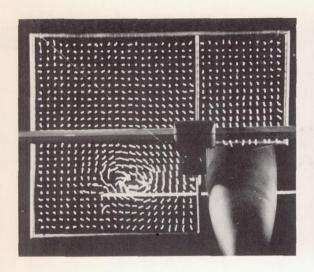
 $x_{TE} = 1.6\overline{c}$ 

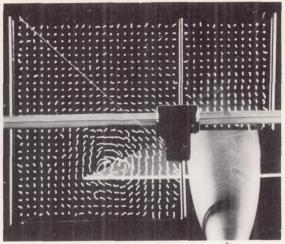


 $x_{TE} = 3.2\overline{c}$ 

(b)  $\alpha_{\rm U} = 10^{\rm O}$ 

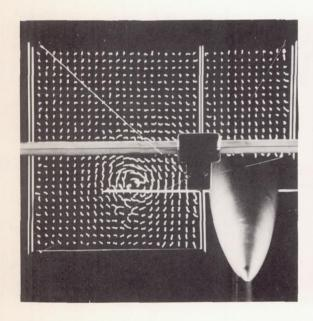
Figure 6.- Continued.

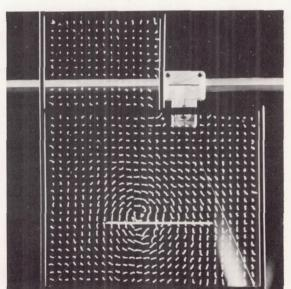




 $x_{TE} = 0.2\overline{c}$ 

 $x_{TE} = 1.0\overline{c}$ 



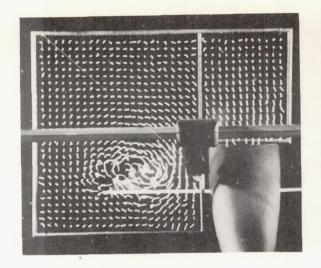


 $x_{TE} = 1.6\overline{c}$ 

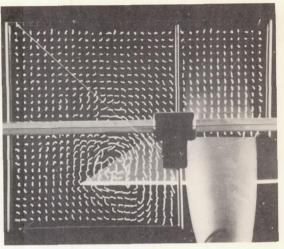
 $x_{TE} = 3.2\overline{c}$ 

(c) 
$$\alpha_{U} = 14^{\circ}$$

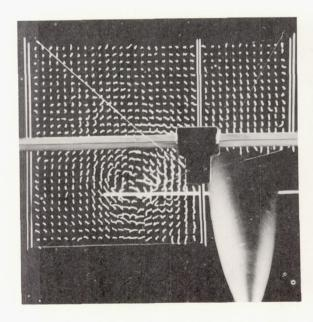
Figure 6.- Continued.



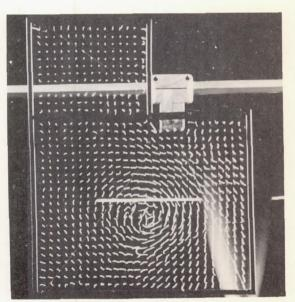
 $x_{TE} = 0.2\overline{c}$ 



 $x_{TE} = 1.0\overline{c}$ 



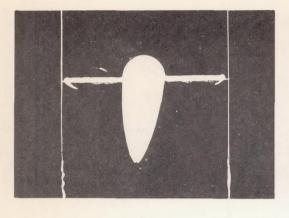
 $x_{TE} = 1.6\bar{c}$ 



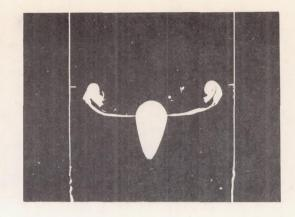
 $x_{TE} = 3.2\overline{c}$ 

(d)  $\alpha_{\rm U} = 20^{\rm O}$ 

Figure 6.- Concluded.



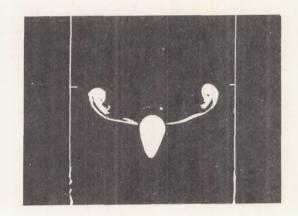
 $x_{TE} = -0.06\bar{c}$ 



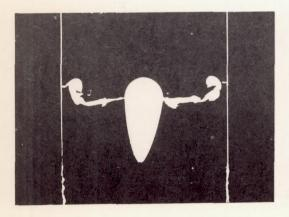
 $x_{TE} = 0.86\bar{c}$ 



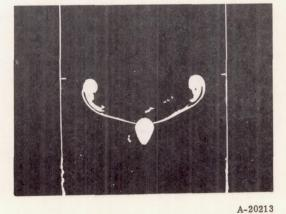
 $x_{TE} = 0.15\overline{c}$ 



 $x_{TE} = 1.13\bar{c}$ 



 $x_{TE} = 0.38\overline{c}$ 



 $x_{TE} = 1.39\bar{c}$ 

Figure 7.- Typical roll-up process of the vortex sheet indicated by white paint deposited on the surface of the water in the water tank;  $\alpha_{\rm u}$  = 20°.

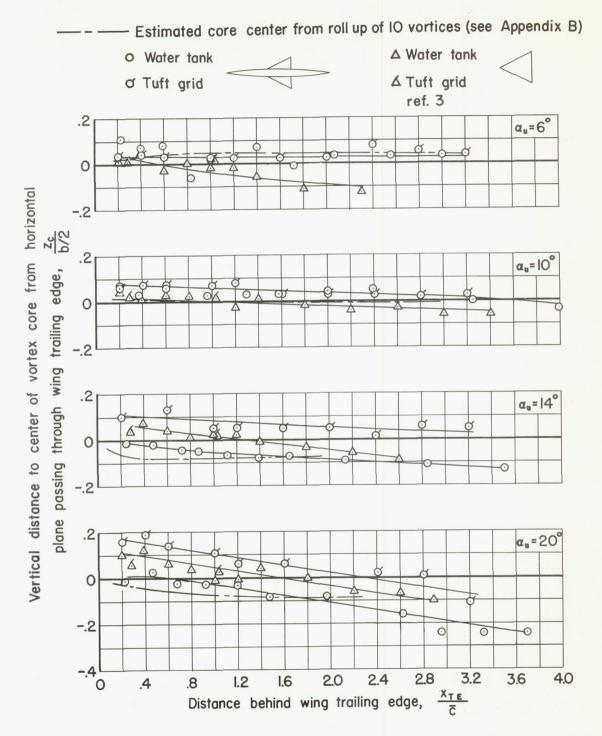


Figure 8.- Variation of the vertical position of the vortex core with longitudinal distance behind the wing trailing edge.

E

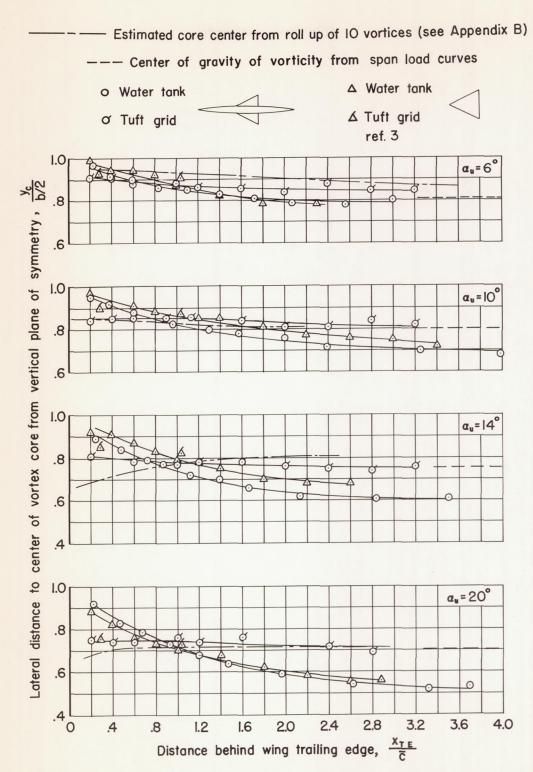


Figure 9.- Variation of the lateral position of the vortex core with longitudinal distance behind the wing trailing edge.